Modern Physics Letters B
2150278 (19 pages)

DOI: 10.1142/s021798492150278X

Joule heating, activation energy and modified diffusion analysis for 3D slip flow of tangent hyperbolic nanofluid with gyrotactic microorganisms

Yu-Ming Chu

Department of Mathematics, Huzhou University, Huzhou 313000, China
Hunan Provincial Key Laboratory of Mathematical, Modeling and Analysis in Engineering, Changsha University of Science and Technology, Changsha 410114, China

Hassan Waqas, Sajjad Hussain and Sumeira Yasmein

Department of Mathematics, Government College University Faisalabad, 31200 Layyah Campus, Pakistan

Sami Ullah Khan

Department of Mathematics, COMSATS University, Islamabad, Sahiwal 57000, Pakistan

M. Ijaz Khan*

Department of Mathematica and Statistics, Riphah International University I-14, Islamabad 44000, Pakistan
ijazfmg_khan@yahoo.com

S. Kadry

Department of Mathematics and Computer Science, Beirut Arab University, Beirut, Lebanon

Received 25 November 2020
Revised 13 January 2021
Accepted 28 January 2021
Published 00 April 2021

Current communication aims to examine the novel thermal consequences of thermal radiation, Joule heating and activation energy in bioconvection flow of tangent hyperbolic nanofluid. The flow is developed by a three-dimensional (3D) extending surface in presence of porous space. The heat and mass transfer inspection in non-Newtonian fluid flow is inspected in laws of modified flux relations. The Brownian movement and thermophoresis diffusions are also accounted for current analysis. The governing formulated frameworks are simplified by appropriate similarity transformations. A familiar shooting scheme for obtaining the numerical outcomes to the nonlinear system is carried out. The graphical results are obtained with the aid of shooting technique. Flow of

*Corresponding author.

fluid, thermal field, concentration of species and microorganism's field are conducted for tangent hyperbolic fluid. Furthermore, the significance of various noteworthy variables on velocity field, thermal field, solutal field of nanomaterials, microorganisms' profile, local skin friction coefficients, local heat flux rate, local Sherwood number and local microorganisms density number is scrutinized in graphical and tabular structure. The importance of current model is in the field of nanotechnology and bioengineering.

Keywords: Hyperbolic tangent nanofluid; bioconvection; Cattaneo–Christov double diffusion theory; shooting scheme.

1. Introduction

The homogeneous suspension of nanometer-sized rigid materials and base fluids is called nanofluid. A novel method for enhancing the efficiency and performance of heat exchangers is the suspension of nanometer-sized particles in standard fluids. In particular, nanomaterials are assumed to derive their characteristics through nanoparticles. In general, non-materials have a large surface-to-volume ratio that is ideal for successful nanoliquid mass transmission rate. Basically, due to their low thermal efficiency, these operating liquids contain low heat transfer characteristics. Therefore, the use of solid particles in this form of working fluid is a very charismatic way of improving the heat conductivity of certain fluids. These non-materials are specifically made of metals, oxidation ceramics, carbon steel and several certain composite materials. Nanofluids are interesting in different industrial applications, especially in refrigeration, smaller process, regional technology, heat ex-changers as well as auto-motives, respectively. In addition, nanofluid plays a key role in meeting the requirements of superior temperature efficiency cooling speeds. Analyses about nanofluid implementations have obtained more interest in recent years owing to their potential application to increase thermal properties of liquid in the cooling of solar technologies. Applications of the nanoliquid have shown huge potential for heat transport in different systems. Anywhere and everywhere energy devices are involved, they are small in size. Cancer treatment with medical treatment, wound treatment, physiological condition, reactivating of arteries and operations, respectively, is optimistic about the use of nanoliquid. The main characteristics of nanoliquid are sufficient storage of heat radiation and larger coefficients of convective thermal transport. In the initial periods, simple fluids such as water, oil, respectively, have been used for heat conduction as well as heat transfer, which have very low heat conductivity. Eventually, in 1995, with the development of nanotechnology, Chinese scholars Choi *et al.*[1] presented a new fluid named nanofluid. They experimentally checked that nanoliquid exhibits comparatively greater thermal conductivity and heat transmission rate efficiencies than easy or basic liquids used during various equipment. Buongiorno[2] used this concept of nanoliquid to build a mathematical structure that could promote the investigation and study of the thermal properties of liquids and the concentration of nanometer size-particles in base liquids. Ramzan *et al.*[3] explained the three-dimensional (3D) dusty nanofluid thin film flowing through nonlinear thermal radiation over

an inclined spinning disc at constant angular velocity of Ω. Tlili *et al.*[4] illustrated the 3D Maxwell nanoliquid magneto hydrodynamic flow through heat Effects of absorbing/generation. Ahmad *et al.*[5] recognized the unstable 3D flow of 2nd-grade nanoliquid owing to thermophoresis motion impacts. Khan *et al.*[6] scrutinized the magnetohydrodynamic flow of asymmetrically nanofluid. The thermal efficiency of Al2O3/water nanoliquid flows across a rectangular microchannel heat sink with uniform heat flux was analyzed by Kahani, *et al.*[7] Ali *et al.*[8] manifested the thermal radiation as well as heat generation/incorporation aspects in flow of viscous nanoliquid. The properties of a hybrid nanofluid flow via an isothermal warmed horizontal tube are examined by Benkhedda *et al.*[9] Ghahremanian *et al.*[10] observed the influence of nanomaterials on the annular movement of Argon-Copper evaporation nanofluid moving through the nanochannel by a molecular dynamic process. Amini *et al.*[11] described the thermal transfer in a microchannel including a harmonic revolving longitudinal vortex generation is implemented. In Bahiraei *et al.*, Ref. 12, the consequences of water — boehmite alumina nanoliquid with different type of nanoparticles via second law properties of the microchannel heat sink are evaluated. Roşca *et al.*[13] scrutinized the nanofluid flow through stretching/shrinking cylinder in porous medium. Mathematical study of Eyring–Powell nanoliquid in 3-dimensions nonlinear heat transfer with improved heat plus mass fluxes is researched by Muhammad *et al.*[14] Ali *et al.*[15] observed the performance of the expansion-contracting cylinder for the cross-fluid flow of non-materials in a magnetic system. Taza *et al.*[16] examined the magnetic dipole effect of the hybrid nanoliquid flowing over the expanding sheet. Eid *et al.*[17] investigated the boundary-layer flow of Carreau nanofluid across a non-linearly stretching surface. Ogunseye *et al.*[18] explored the entropy production of the viscous hybrid nanoliquid defined in the Eyring–Powell method. Faisal *et al.*[19] analyzed the properties magnetized flow of Casson nanofluid induced by bi-directionally stretching surface in porous channel.

Swante Arrhenius was the principal in 1889, who began the discussion about activation energy, and there is a minimal amount of energy needed to control the reactants to a situation from which they can encounter substance improvement. The application includes compound construction, maintenance handling, transport methods, geothermal stores as well as enterprises. Heat and mass transportation types handle various systems that are synthetically reacting to species compound reactions alongside implementation vitality applied to oil supply or geothermal architecture. Activation energy plays an important role in chemical processes, as this element is important in the usage of geothermal reservoir manufacturing, oil emulsification and chemistry of water. The concept of activation energy was originally introduced by Arrhenius.[20] He explained that the least amount of energy (or minimum energy) needed to work atoms and molecules in a chemical process are needed to start a chemical process. A basic model including boundary layer liquid flow problems under the binary chemical process with Arrhenius activation energy was first described by Bestman.[21] In natural convection, he used a disturbance approach to

understand the effect of the activation energy. Currently, many researchers work on activation energy model is presented in Refs. 22–25.

Bioconvection is a process that happens when, on average, motile microorganisms that are heavier than the liquid atmosphere swim upwards, producing a density instability that induces fluid movement. This accumulation of upward-moving cells at down welling sites has similarity to the concentration of buoyant substance that passively travels upward at down welling sites in the Langmuir process. After all, although the circulation of Langmuir allows the buoyant substance to be passively aggregated, in gyrotactic microorganisms it is the active swimming of the microorganisms which both drives the movement and allows the cells to transfer upwards. So, several single-celled bacteria have the ability to experience bioconvection; algae cells are usually denser than their liquid environment and often swimming upwards, for instance because they are low strong or they're just phototactic. In the experiment, falling plumes or cell streams are sometimes shown in culture flasks, an instance of gyrotactic microorganisms. The term "bioconvection" was first described in the study of James Henry Platt in order to draw the interest of several other investigators to the physics of streaming patterns found in dense environments of free-swimming motile organisms. According to Platt,[26] the transforming polygonal structures in dense Tetrahymena cultures (i.e. ciliate as well as flagellate) such as "Benard cells" do not owe to heat convection. There are several bacteria (microbes) and it is well established that several bacteria can be destroyed and often killed when exposed to higher temperatures. Thermopile, on the other hand, is an organism usually involved in different heated areas of the earth. Internal flow via a porous medium with an extension/stretching wall has a few essential applications in biochemical flows, including blood flow and experimental dialysis, air and blood movement in the circulatory system. Additional applications include tissue filtration, oxygen absorption in capillaries, industrialized of cosmetic products, cochlea mechanisms in the human ear, swirling diaphragms. The concept of bioconvection of nanoliquid with gyrotactic motile microorganisms was introduced by Kuznetsov.[27] Sohail *et al.*[28] addressed the entropy assessment of the gyrotactic motile Microorganism-consisting Maxwell nanofluid. Bhatti *et al.*[29] analyzed Arrhenius activation energy through thermo-bioconvection nanoliquid via Riga plate. Khan *et al.*[30] observed bioconvection in nanofluid through two stretching rotating discs including entropy generation. Waqas *et al.*[31] visualized second-grade nanoliquid flow with gyrotactic microorganisms through stretched surfaces. Khan *et al.*[32] represented the manufacture of nanobiomaterials and the improvement of heat extrusion systems are based upon on rheology of couples stress nanoliquid under the effects of activation energy, porous media, heat transfer, gyrotactic motile micro-organisms as well as convective boundary conditions. Waqas *et al.*[33] examined the bioconvection aspects in nanofluid flow. Many investigators worked on bioconvection flow of nanofluid with gyrotactic motile microorganisms, see in Refs. 34–40.

This investigation aims to analyze the novel consequences of Joule heating, thermal radiation and activation energy in 3D flow of tangent hyperbolic nanofluid induced by a bi-directional surface. The most generalized diffusion expressions (Cattaneo–Christov laws) are utilized to analyze the heat and mass transfer phenomenon. The resulting problem based on such improved thermal features is numerically solved by employing shooting technique. The fundamental physical influence of non-Newtonian thermal model is reported via several graphs.

2. Formulation of Flow Problem

2.1. *Flow modeling*

Consider a 3D magnetized hyperbolic tangent nanofluid containing microorganisms over a porous extending surface with Cattaneo–Christov heat/mass diffusion theory, as depicted in Fig. 1. The behavior of nonlinear thermal radiation is also discussed. The joule heating aspects, activation energy and heat sink/source are conducted in a porous medium. The surface is extending with velocities $u_w(x) = ax$ and $v_w(y) = by$ in the direction of x- and y-axis, respectively. Furthermore, here in the case of extending surface $b > 0$ while for shrinking surface $b < 0$.

Under the above consideration, governing equations can be written as follows:

$$\frac{\partial u}{\partial x} + \frac{\partial v}{\partial y} + \frac{\partial w}{\partial z} = 0, \tag{1}$$

$$u\frac{\partial u}{\partial x} + v\frac{\partial u}{\partial y} + w\frac{\partial u}{\partial z} = \nu(n-1)\frac{\partial^2 u}{\partial z^2} + \nu n\sqrt{2}\Gamma\frac{\partial u}{\partial z}\left(\frac{\partial^2 u}{\partial z^2}\right) - \frac{\sigma^* B_0^2}{\rho_f}u - \frac{\nu}{K_1}u + \frac{1}{\rho_f}\begin{bmatrix}(1-C_f)\rho_f\beta^{**}g*(T-T_\infty) - (\rho_p-\rho_f)g^*(C-C_\infty) \\ -(N-N_\infty)g^*\gamma(\rho_m-\rho_f)\end{bmatrix}, \tag{2}$$

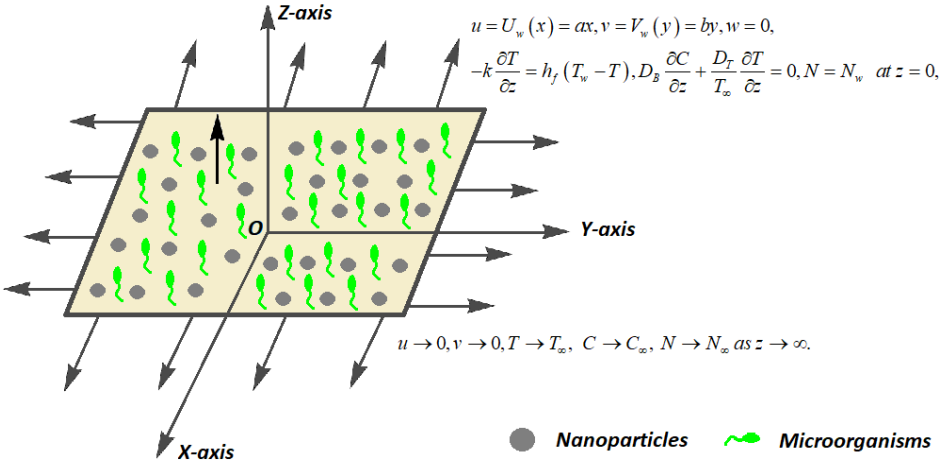

Fig. 1. (Color online) The flow configuration.

$$u\frac{\partial v}{\partial x}+v\frac{\partial v}{\partial y}+w\frac{\partial v}{\partial z}=\nu(n-1)\frac{\partial^2 v}{\partial z^2}+n\nu\sqrt{2}\Gamma\frac{\partial v}{\partial z}\frac{\partial^2 v}{\partial z^2}-\frac{\sigma^* B_0^2}{\rho_f}v-\frac{\nu}{K_1}v, \tag{3}$$

$$\begin{aligned}
&u\frac{\partial T}{\partial x}+v\frac{\partial T}{\partial y}+w\frac{\partial T}{\partial z}+\Gamma_E\\
&\qquad\times\left[\begin{array}{l}
u^2\dfrac{\partial^2 T}{\partial x^2}+v^2\dfrac{\partial^2 T}{\partial y^2}+w^2\dfrac{\partial^2 T}{\partial z^2}+2uv\dfrac{\partial^2 T}{\partial x\partial y}+2vw\dfrac{\partial^2 T}{\partial y\partial z}\\
\quad+2uw\dfrac{\partial^2 T}{\partial x\partial z}+\left(u\dfrac{\partial u}{\partial x}+v\dfrac{\partial u}{\partial y}+w\dfrac{\partial u}{\partial z}\right)\dfrac{\partial T}{\partial x}\\
\quad+\left(u\dfrac{\partial v}{\partial x}+v\dfrac{\partial v}{\partial y}+w\dfrac{\partial v}{\partial z}\right)\dfrac{\partial T}{\partial y}+\left(u\dfrac{\partial w}{\partial x}+v\dfrac{\partial w}{\partial y}+w\dfrac{\partial w}{\partial z}\right)\dfrac{\partial T}{\partial z}
\end{array}\right]\\
&\quad=\left(\alpha+\frac{1}{(\rho c)_p}\frac{16\sigma^* T_\infty^3}{3k^*}\right)\frac{\partial T}{\partial z}+\tau\left\{D_B\frac{\partial C}{\partial z}\frac{\partial T}{\partial z}+\frac{D_T}{T_\infty}\left(\frac{\partial T}{\partial z}\right)^2\right\}+\frac{\sigma^* B_0^2}{\rho c_p}u^2\\
&\qquad+\frac{Q_0}{\rho c_p}(T-T_\infty)+\frac{\nu}{c_p}(1-n)\left(\frac{\partial u}{\partial z}\right)^2,
\end{aligned} \tag{4}$$

$$\begin{aligned}
&u\frac{\partial C}{\partial x}+v\frac{\partial C}{\partial y}+w\frac{\partial C}{\partial z}+\Gamma_C\\
&\qquad\times\left[\begin{array}{l}
u^2\dfrac{\partial^2 C}{\partial x^2}+v^2\dfrac{\partial^2 C}{\partial y^2}+w^2\dfrac{\partial^2 C}{\partial z^2}+2uv\dfrac{\partial^2 C}{\partial x\partial y}+2vw\dfrac{\partial^2 C}{\partial y\partial z}\\
\quad+2uw\dfrac{\partial^2 C}{\partial x\partial z}+\left(u\dfrac{\partial u}{\partial x}+v\dfrac{\partial u}{\partial y}+w\dfrac{\partial u}{\partial z}\right)\dfrac{\partial C}{\partial x}\\
\quad+\left(u\dfrac{\partial v}{\partial x}+v\dfrac{\partial v}{\partial y}+w\dfrac{\partial v}{\partial z}\right)\dfrac{\partial C}{\partial y}+\left(u\dfrac{\partial w}{\partial x}+v\dfrac{\partial w}{\partial y}+w\dfrac{\partial w}{\partial z}\right)\dfrac{\partial C}{\partial z}
\end{array}\right]\\
&\quad=D_B\left(\frac{\partial^2 C}{\partial z^2}\right)+\frac{D_T}{T_\infty}\left(\frac{\partial^2 T}{\partial z^2}\right)-Kr^2(C-C_\infty)\left(\frac{T}{T_\infty}\right)^m\exp\left(\frac{-E_a}{K_1 T}\right),
\end{aligned} \tag{5}$$

$$u\frac{\partial N}{\partial x}+v\frac{\partial N}{\partial y}+w\frac{\partial N}{\partial z}+\left[\frac{\partial}{\partial z}\left(N\frac{\partial C}{\partial z}\right)\right]\frac{bW_c}{(C_w-C_\infty)}=D_m\frac{\partial}{\partial z}\left(\frac{\partial N}{\partial z}\right), \tag{6}$$

with boundaries constraints

$$\left.\begin{array}{l}
u=U_w(x)=ax,\ v=V_w(y)=by,\ w=0,\\
-k\dfrac{\partial T}{\partial z}=h_f(T_w-T),\ D_B\dfrac{\partial C}{\partial z}+\dfrac{D_T}{T_\infty}\dfrac{\partial T}{\partial z}=0,\ N=N_w \text{ at } z=0,\\
u\to 0,\ v\to 0,\ T\to T_\infty,\ C\to C_\infty,\ N\to N_\infty\ asz\to\infty,
\end{array}\right\} \tag{7}$$

where u, v and w are components of velocity in the direction x, y and z, respectively, g^* signifies the gravity, ρ_m for the microorganism density, ρ_p is the density of nanoparticles, ν stand for kinematic viscosity, thermal diffusivity is denoted by α, D_B for coefficient of Brownian diffusion (T, C, N) denotes temperature, concentration and microorganisms correspondingly, Γ_E, and Γ_C are the relaxation time

of heat and mass fluxes, respectively, m is fitted rate constant, Kr^2 depicts the coefficient of chemical reaction rate, D_T is thermophoresis diffusion coefficients and D_m is the coefficient of microorganisms coefficient.

The following suitable dimensionless variables are specified in order to reduce governing system of PDEs to nonlinear dimensionless ordinary differential equations:

$$\left.\begin{aligned} &u = axf'(\zeta),\ v = ayg'(\zeta),\ w = -\sqrt{a\nu}[f(\zeta)+g(\zeta)],\\ &\theta(\zeta) = \frac{T-T_\infty}{T_w-T_\infty},\ \varphi(\zeta) = \frac{C-C_\infty}{C_w-C_\infty},\ \chi(\zeta) = \frac{N-N_\infty}{N_w-N_\infty},\ \zeta = z\sqrt{\frac{a}{\nu}}. \end{aligned}\right\} \tag{8}$$

Invoking appropriate similarity transformation (10), Eq. (1) is verified trivially and expressions (2)–(6) are transformed to

$$f'''[(1-n)+n\mathrm{We}_1 f''] - f'^2 + f''(f+g) - Mf' - Kf' + \lambda(\theta - \mathrm{Nr}\phi - Nc\chi) = 0, \tag{9}$$

$$(f+g)g'' - g'^2 + g'''[(1-n)+n\mathrm{We}_2 f''] - Mg' - Kg' = 0, \tag{10}$$

$$\left[1+\frac{4}{3}\mathrm{Rd}\right]\theta'' + \mathrm{Pr}(f+g)\theta' + \mathrm{PrNb}\theta'\phi' + \mathrm{PrNt}(\theta')^2 + \mathrm{ME}cf'^2 + \mathrm{Pr}\,Q\theta + (1-n)\mathrm{Ec}f''^2 - \mathrm{Pr}\,\Omega_T[(f+g)(f'+g')\theta' + (f+g)^2\theta''] = 0, \tag{11}$$

$$\phi'' + \mathrm{Le}\,\mathrm{Pr}(f+g)\phi' + \frac{\mathrm{Nt}}{\mathrm{Nb}}\theta'' - \mathrm{Le}\,\mathrm{Pr}\,\sigma(1+\delta\theta)^n \exp\left(\frac{-E}{1+\delta\theta}\right)\phi - \mathrm{Le}\,\mathrm{Pr}\,\Omega_C[(f+g)(f'+g')\phi' + (f+g)^2\phi''] = 0, \tag{12}$$

$$\chi'' + \mathrm{Lb}(f+g)\chi' - \mathrm{Pe}[\chi'\phi' + (\Omega+\chi)\phi''] = 0. \tag{13}$$

With restrictive conditions

$$\left.\begin{aligned} &f'(0) = 1,\ g'(0) = \alpha,\ g(0) = 0,\ \theta'(0) = -\mathrm{Bi}(1-\theta(0)),\\ &\varphi'(0) + \frac{\mathrm{Nt}}{\mathrm{Nb}}\theta'(0) = 0,\ \chi(0) = 1,\\ &f'(\infty) = 0,\ g'(\infty) = 0,\ \theta(\infty) = 0,\ \varphi(\infty) = 0,\ \chi(\infty) = 0. \end{aligned}\right\} \tag{14}$$

Here, Weissenberg numbers are expressed by $\mathrm{We}_1 = \sqrt{2\frac{a}{\nu}}a\Gamma x$ and $\mathrm{We}_2 = \sqrt{2\frac{a}{\nu}}a\Gamma y$, $M = \frac{\sigma^* B_0^2}{a\rho}$ is Hartmann number, porosity parameter is characterized as $K = \frac{\nu}{aK_1}$, velocity slip parameters are $\delta_1 = \sqrt{a\alpha}N_2$ and $\delta_2 = \sqrt{a\alpha}N_2$, rotation parameter is $\alpha = \frac{b}{a}$, Mixed convection parameter symbolized by $\lambda = \frac{\beta^{**}g*(1-C_\infty)(T_w-T_\infty)}{aU_w}$, the plate is impermeable, $\mathrm{Nr} = \frac{(\rho_p-\rho_f)(C_w-C_\infty)}{\rho_f(1-C_\infty)(T_w-T_\infty)\beta^{**}}$ perform the Buoyancy ratio parameter, Bioconvection Rayleigh number is symbolized by $\mathrm{Nc} = \frac{\gamma*(\rho_m-\rho_f)(N_w-N_\infty)}{\rho_f(1-C_\infty)(T_w-T_\infty)\beta^{**}}$, $\mathrm{Nb} = \frac{\tau D_B(C_w-C_\infty)}{\nu}$ the Brownian parameter, $\mathrm{Nt} = \frac{\tau D_T(T_w-T_\infty)}{\nu T_\infty}$, Radiation parameter is $\mathrm{Rd} = \frac{4\sigma^* T_\infty^3}{3k^*k}$, $\mathrm{Pr} = \frac{\nu}{\alpha}$ the Prandtl number, Eckert number is $\mathrm{Ec} = \frac{u_w^2}{c_p(T_w-T_\infty)}$, chemical reaction parameter is $\sigma = \frac{Kr^2}{a}$,

Le $= \frac{\alpha}{D_B}$ the Lewis number, $E = \frac{E_a}{K_1 T_\infty}$, the activation energy parameter, radiation parameter Rd $= \frac{4\sigma T_\infty^3}{k^* k}$, heat generation/absorption parameter is $Q = \frac{Q_0}{a\rho c_p}$, thermal relaxation and concentration relaxation parameters are $\Omega_T = a\Gamma_E$ and $\Omega_C = a\Gamma_C$, respectively, bioconvection Lewis number is denoted by Lb $= \frac{\nu}{D_m}$, Peclet number is read as Pe $= \frac{bW_c}{D_m}$, microorganisms difference variable is denoted by $\Omega = \frac{N_\infty}{N_w - N_\infty}$ while Bi $= \frac{h_f}{k}\sqrt{\frac{\nu}{a}}$ stands for Biot number.

2.2. *Physical quantities of interest*

The wall shear stress for current non-Newtonian model is defined as

$$C_{fx} = \frac{\tau_{wx}}{\rho U_w^2}, \quad C_{fy} = \frac{\tau_{wy}}{\rho V_w^2}, \tag{15}$$

which is in dimensionless form

$$\left.\begin{aligned} \left(\frac{\mathrm{Re}_x}{\mathrm{Pr}}\right)^{0.5} C_{fx} &= \left[(1-n)f''(0) + \frac{n\mathrm{We}_x}{2} f''^2(0)\right], \\ \left(\frac{\mathrm{Re}_y}{\mathrm{Pr}}\right)^{0.5} (\lambda)^{\frac{3}{2}} C_{fy} &= \left[(1-n)g''(0) + \frac{n\mathrm{We}_y}{2} g''^2(0)\right]. \end{aligned}\right\} \tag{16}$$

Similarly the local Nusselt number, local Sherwood number and motile density number are

$$\mathrm{Nu}_x = \frac{xq_w}{k(T_w - T_\infty)}, \quad \mathrm{Sh}_x = \frac{xq_m}{D_B(C_w - C_\infty)}, \quad \mathrm{Sn}_x \frac{xq_n}{D_m(N_w - N_\infty)}, \tag{17}$$

where

$$q_w = -k\left(\frac{\partial T}{\partial z}\right)_{z=0}, \quad q_m = -D_B\left(\frac{\partial C}{\partial z}\right)_{z=0}, \quad q_n = -D_m\left(\frac{\partial N}{\partial z}\right)_{z=0}. \tag{18}$$

In dimensionless form

$$\left.\begin{aligned} \mathrm{Nu}_x &= -\left(1 + \frac{4}{3}\mathrm{Rd}\right)(\mathrm{Pr}\,\mathrm{Re}_x)^{1/2}\theta'(0), \\ \mathrm{Sh}_x &= -(\mathrm{Pr}\,\mathrm{Re}_x)^{1/2}\varphi'(0), \\ \mathrm{Sn}_x &= -(\mathrm{Re}_x)^{1/2}\chi'(0), \end{aligned}\right\} \tag{19}$$

where $\mathrm{Re}_x = \frac{xu_w}{\nu}$ and $\mathrm{Re}_y = \frac{yv_w}{\nu}$ are Reynolds number for bio-directional moving surfaces.

3. Numerical Approach

To accurately clarify the arrangement of ODEs is not easily amenable owing to nonlinearity character. The above-mentioned combined ordinary differential equations (11)–(15) with the related boundary restrictions (16)–(17) are constructed using the MATLAB computational computer-language bvp4c shooting technique.

Bvp4c is effectively a Lobattao-IIIa collocation formula which is used for a numerical analysis. The higher order differential method is discretized into first-order ODE, and the use of sufficient variables is described as follows.

Let

$$\begin{aligned}
&f = s_1, \quad f' = s_2, \quad f'' = s_3, \quad f''' = s_3', \\
&g = s_4, \quad g' = s_5, \quad g'' = s_6, \quad g''' = s_6', \\
&\theta = s_7, \quad \theta' = s_8, \quad \theta'' = s_8', \\
&\phi = s_9, \quad \phi' = s_{10}, \quad \phi'' = s_{10}', \\
&\chi = s_{11}, \quad \chi' = s_{12}, \quad \chi'' = s_{12}',
\end{aligned} \tag{20}$$

$$s_3' = \frac{s_2^2 - s_3(s_1 + s_4) + Ms_2 + Ks_2 - A^*(s_7 - \mathrm{Nr}s_9 - \mathrm{Nc}s_{11})}{[(1-n) + n\mathrm{We}_x s_3]}, \tag{21}$$

$$s_6' = \frac{-(s_1 + s_4)s_6 + s_5^2 + Ms_5 + Ks_5}{[(1-n) + n\mathrm{We}_y s_3]}, \tag{22}$$

$$s_8' = \frac{\begin{array}{c} -\Pr(s_1 + s_4)s_8 - \mathrm{PrNb}s_8 s_{10} - \mathrm{PrNt}(s_8)^2 - \mathrm{ME}cs_2^2 \\ -\Pr Qs_7 - (1-n)\mathrm{Ec}s_3^2 + \Pr\Lambda_T[(s_1 + s_4)(s_2 + s_5)s_8] \end{array}}{\left[\left[1 + \frac{4}{3}\mathrm{Rd}\right] - \Pr\Lambda_T(s_1 + s_4)^2\right]}, \tag{23}$$

$$s_{10}' = \frac{\begin{array}{c} -\mathrm{Le}\Pr(s_1 + s_4)s_{10} - \dfrac{\mathrm{Nt}}{\mathrm{Nb}}s_8' + \mathrm{Le}\Pr\sigma(1 + \delta s_7)^n \exp\left(\dfrac{-E}{1 + \delta s_7}\right)s_9 \\ +\mathrm{Le}\Pr\Lambda_C[(s_1 + s_4)(s_2 + s_5)s_{10}] \end{array}}{[1 - \mathrm{Le}\Pr\Lambda_C(s_1 + s_4)^2]}, \tag{24}$$

$$s_{12}' = -\mathrm{Lb}(s_1 + s_4)s_{12} + \mathrm{Pe}[s_{12}s_{10} + (\Omega + s_{11})s_{10}']. \tag{25}$$

Through restrictive conditions

$$\begin{aligned}
&s_2(0) = 1, \quad s_5(0) = \alpha, \quad s_4(0) = 0, \quad s_8(0) = -\mathrm{Bi}(1 - s_7(0)), \\
&s_{10}(0) + \frac{\mathrm{Nt}}{\mathrm{Nb}}s_8(0) = 0, \quad s_{11}(0) = 1,
\end{aligned} \tag{26}$$

$$s_2(\infty) = 0, \quad s_5(\infty) = 0, \quad s_7(\infty) = 0, \quad s_9(\infty) = 0, \quad s_{11}(\infty) = 0. \tag{27}$$

4. Discussion

In this section, the main importance of this paper is to explore the properties of 3D radiative flow of hyperbolic tangent nanofluid over an extending surface in the presence of activation energy and convective boundary condition. The aim of this section is to focus under the attained numerical result associated to the velocity profiles f' and g', thermal distribution θ, nanoparticles concentration field ϕ, and motile microorganisms field χ for the important involved parameters like Hartmann number M, power law index parameter n, constant parameter of sheet λ, Weissenberg

number We_1, mixed convection parameter λ, buoyancy ratio parameter Nr, bioconvection Rayleigh number Nc, Weissenberg number We_2, rotation parameter α, Prandtl number Pr, temperature ratio parameter θ_w, thermal relaxation parameter Ω_T, concentration relaxation parameter Ω_C, activation energy parameter E, Lewis number Le, Brownian motion parameter Nb, thermophoresis parameter Nt, Biot number Bi, Peclet number Pe and bioconvection Lewis number Lb that are displayed in Figs. 2–16.

In this part, the influence of prominent parameters M, n, λ, We_1, Nr, Nc, We_2 and, α against velocity distributions f' and g' has been interpreted in Figs. 2–6. Figure 2 highlights the impact of Hartmann number M and power law index parameter n over velocity field f'. It can be noticed that the augmentation of magnetic pa Hartmann number M causes diminishes the velocity of fluid f', and also observed that enhancement value of power law index parameter n causes reduction in velocity distribution f'. Physically, this is owing to the magnetic field provided that a retarding body force recognized as the Lorentz force, which acts transversely in the way of the industrial magnetic field. The flow of the boundary layer and the

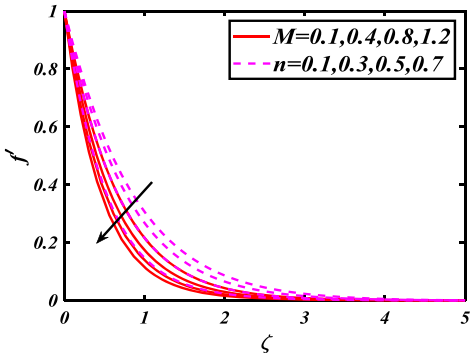

Fig. 2. (Color online) Dependence of f' against M and n.

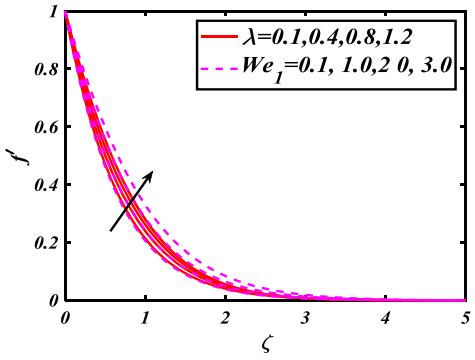

Fig. 3. (Color online) Dependence of f' against λ and We_1.

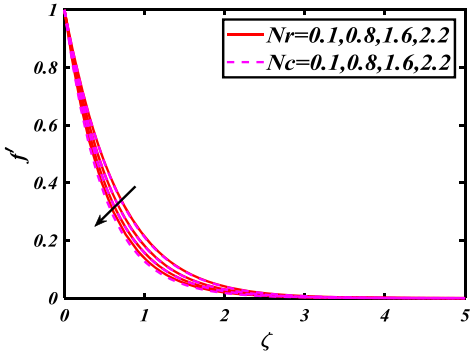

Fig. 4. (Color online) Dependence of f' against Nr and Nc.

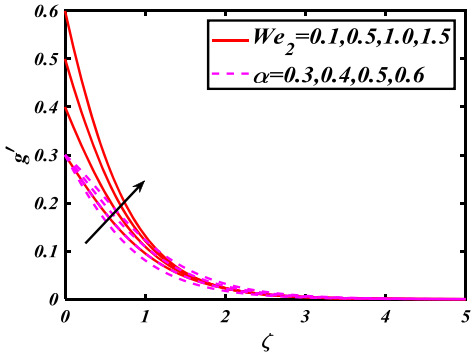

Fig. 5. (Color online) Dependence of g' against We_2 and α.

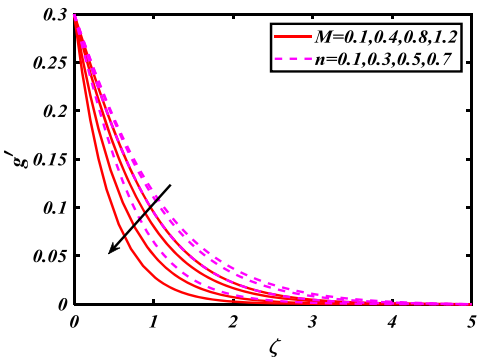

Fig. 6. (Color online) Dependence of g' against M and n.

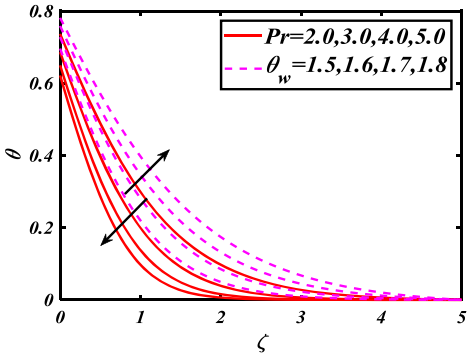

Fig. 7. (Color online) Dependence of θ against Pr and θ_w.

thickness of the boundary layer of momentum are declined by the body force. Also, owing to the resistive force, a fractional resistor force that opposes liquid flow motion, it produced heat. Figure 3 portrays the variation of mixed convection parameter λ as well as Weissenberg number We_1 via velocity of tangent hyperbolic fluid f'. As expected, it is clear that the velocity distribution f' boost due to enlarged mixed convection parameter λ. Also it is clear that increasing value of Weissenberg number We_1 causes augmentation in the velocity field f'. Figure 4 delineates the characteristics of buoyancy ratio parameter Nr and bioconvection Rayleigh number Nc against velocity of fluid f'. Since inspected, it is noticed that with higher value of buoyancy ratio parameter Nr and bioconvection Rayleigh number Nc the flow of fluid f' is reduced. Figure 5 elucidates the influence of Weissenberg number We_2 and rotation parameter α over velocity field g'. Generally, it is observed that rising magnitudes of Weissenberg number We_2 enhanced the velocity distribution g'. Also with the increment of rotation parameter α enhanced the velocity distribution g'. The impact of Hartmann number M and power law index parameter n via velocity field g' is portrayed through Fig. 6. From this figure, it is clear that for boosted value of Hartmann number M the velocity distribution g' decreased and also observed that the raising value of the power law index parameter n causes the reduction in velocity distribution g'. Impacts of prominent parameters including Pr, θ_w, Nt, Bi, Ω_T, λ over thermal field of nanoparticles θ are disclosed in Figs.7–10. Figure 7 depicts the impression of Prandtl number Pr and temperature ratio parameter θ_w on thermal distribution θ. It is witnessed that temperature distribution θ diminishes with escalating the values of Prandtl number Pr. On the other hand, the greatest value of temperature ratio parameter θ_w escalates the temperature distribution θ. Figure 8 shows the consequence of thermophoresis parameter Nt and Biot number Bi versus temperature distribution θ. It is analyzed that enlarged value of thermophoresis parameter Nt as well as Biot number Bi causes upsurges in the thermal field of species θ. Figure 9 demonstrates the effect of thermal relaxation parameter Ω_T and mixed convection parameter λ against temperature distribution

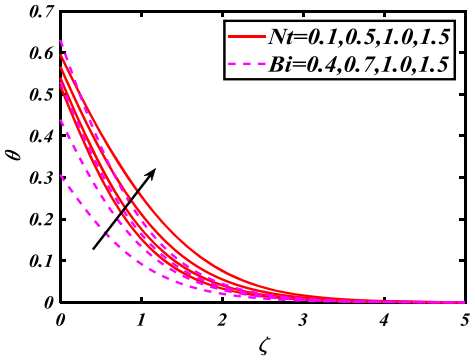

Fig. 8. (Color online) Dependence of θ against Nt and Bi.

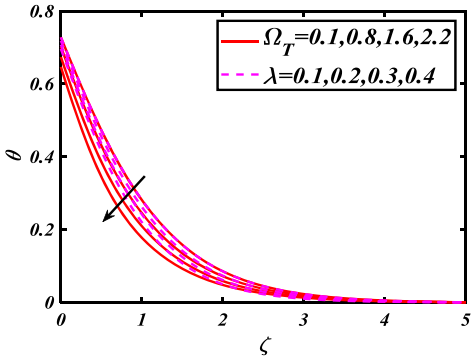

Fig. 9. (Color online) Dependence of θ against Ω_T and λ.

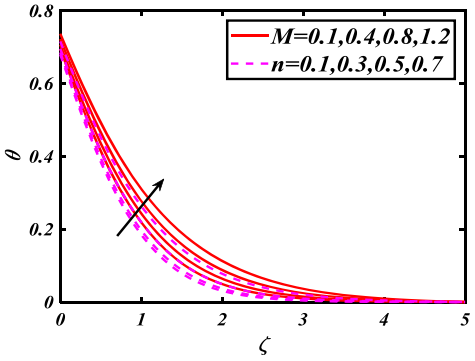

Fig. 10. (Color online) Dependence of θ against M and n.

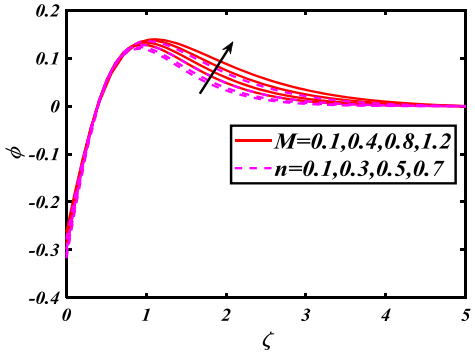

Fig. 11. (Color online) Dependence of ϕ against M and n.

θ. Clearly it is noticed that escalated the variations of thermal relaxation parameter Ω_T causes lower the temperature distribution θ. It is noticed that the growing value of mixed convection parameter λ thermal field θ reduces. Figure 10 represents the inspirations of Hartmann number M and power law index parameter n under the temperature field θ. Generally, it is noted that improving the Hartmann number M escalates the power law index parameter n and causes enhancement in thermal field of bio-nanomaterials θ. The behavior of several impotent parameters like M, n, Ω_C, λ, Nt, E, Nb, Le against concentration field of species ϕ can be seen in Figs. 11–14. Figure 11 is designed to scrutinize the impact of Hartmann number M and power law index parameter n over nanoparticles concentration profile ϕ. It can be noticed that concentration of nanoparticles ϕ exaggerators by improving the value of Hartmann number M and power law index parameter n. Figure 12 is drawn to examine the inspiration of mixed convection parameter λ and concentration relaxation parameter Ω_C versus solutal field of species ϕ. It is noted that lower solutal field of species is developed by using larger mixed convection parameter λ and concentration to relaxation parameter Ω_C. The influence of thermophoresis

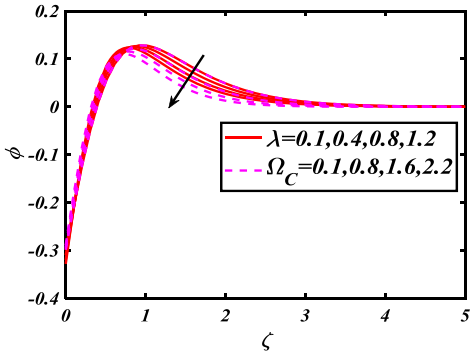

Fig. 12. (Color online) Dependence of ϕ against λ and Ω_C.

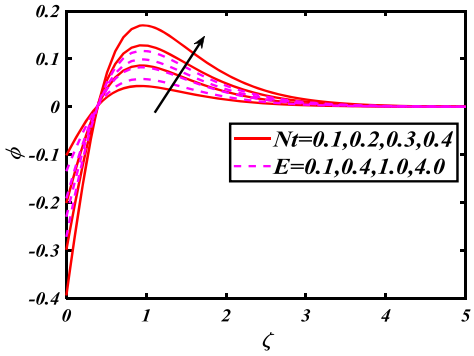

Fig. 13. (Color online) Dependence of ϕ against Nt and E.

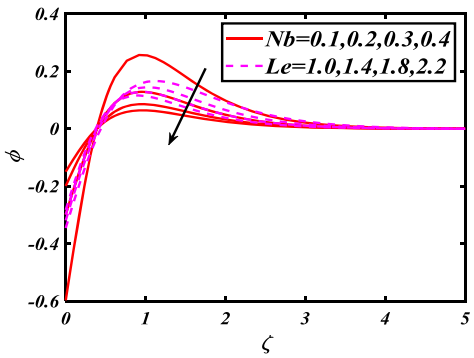

Fig. 14. (Color online) Dependence of ϕ against Nb and Le.

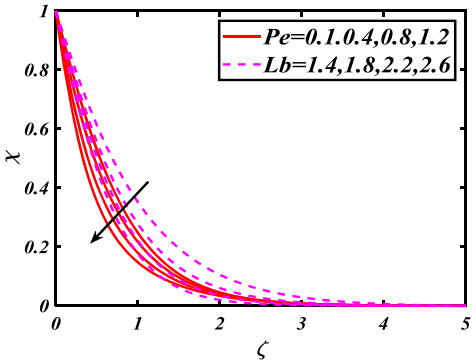

Fig. 15. (Color online) Dependence of χ against Pe and Lb.

parameters Nt and activation energy parameter E on volumetric concentration of nanomaterials ϕ is depicted in Figure 13. It is remarkable that solutal field ϕ of nanoparticles is an enhancing function of thermophoresis parameters Nt and activation energy parameter E. The analogous aspects of Brownian motion parameter Nb and Lewis number Le via concentration of nanoparticles ϕ are portrayed in Fig. 14. Here concentration of nanoparticles ϕ diminishing by increases the value of Brownian motion parameter Nb and Lewis number Le. The effect of some different emerging parameters such as Pe, Lb, M, n, via motile microorganism field χ is displayed in Figs. 15 and 16. The features of Peclet number Pe and bioconvection Lewis number Lb via microorganism field χ are revealed in Fig. 15. From this scenario, it is found that microorganism's field χ declines for larger magnitude of Peclet number Pe and bioconvection Lewis number Lb. Figure 16 is captured to show the outcomes of Hartmann number M and power law index parameter n on microorganism's field χ. It is revealed that larger magnitude of Hartmann number M and power law index parameter n microorganism's field χ upsurges.

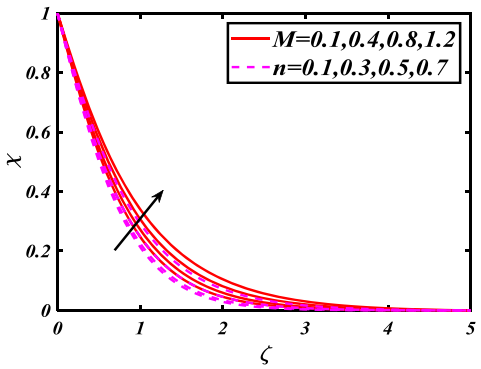

Fig. 16. (Color online) Dependence of χ against M and n.

Table 1. Numerical outcomes of local skin friction coefficients $-f''(0)$, $-g''(0)$ for involved parameters.

Parameters									
λ	Nr	Nc	M	K	α	We_1	We_2	$-f''(0)$	$-g''(0)$
0.2	0.5	0.5	0.5	1.0	0.1	0.3	0.3	1.4292	0.2542
0.6								1.3107	0.2599
1.2								1.1440	0.2672
0.1	0.2	0.5	0.5	1.0	0.1	0.3	0.3	1.4601	0.2526
	0.6							1.4607	0.2531
	1.2							1.4625	0.2541
0.1	0.5	0.2	0.5	1.0	0.1	0.3	0.3	1.4694	0.2520
		0.8						1.5678	0.2543
		1.6						1.6817	0.2565
0.1	0.5	0.5	0.1	1.0	0.1	0.3	0.3	1.4778	0.2534
			0.2					1.4789	0.2621
			0.3					1.4809	0.2707
0.1	0.5	0.5	0.5	2.0	0.1	0.3	0.3	1.4766	0.2545
				3.0				1.4811	0.2623
				4.0				1.4921	0.2678
0.1	0.5	0.5	0.5	1.0	0.2	0.3	0.3	1.4370	0.2612
					0.4			1.3312	0.2506
					0.8			1.1321	0.2475
0.1	0.5	0.5	0.5	1.0	0.1	0.1	0.3	1.4623	0.2634
						0.8		1.4616	0.2577
						1.6		1.4596	0.2494
0.1	0.5	0.5	0.5	1.0	0.1	0.3	0.1	1.4566	0.2656
							0.8	1.4548	0.2631
							1.6	1.4537	0.2596

Table 2. Numerical iteration for mass transfer rate $-\theta'(0)$ versus involved parameters.

Parameters										
λ	Nr	Nc	M	Pr	Nt	Nb	Bi	Ω_T	θ_w	$-\theta'(0)$
0.2	0.5	0.5	0.5	1.2	0.3	0.2	1.0	0.2	0.8	0.4712
0.6										0.4758
1.2										0.4816
0.1	0.2	0.5	0.5	1.2	0.3	0.2	1.0	0.2	0.8	0.4698
	0.6									0.4690
	1.2									0.4674
0.1	0.5	0.2	0.5	1.2	0.3	0.2	1.0	0.2	0.8	0.4693
		0.8								0.4644
		1.6								0.4517
0.1	0.5	0.5	0.1	1.2	0.3	0.2	1.0	0.2	0.8	0.4687
			0.2							0.4656
			0.3							0.4578
0.1	0.5	0.5	0.5	2.0	0.3	0.2	1.0	0.2	0.8	0.5798
				3.0						0.5871
				5.0						0.6188
0.1	0.5	0.5	0.5	1.2	0.1	0.2	1.0	0.2	0.8	0.4792
					0.5					0.4601
					1.2					0.4220
0.1	0.5	0.5	0.5	1.2	0.3	0.1	1.0	0.2	0.8	0.4698
						0.5				0.4699
						1.2				0.4700
0.1	0.5	0.5	0.5	1.2	0.3	0.2	0.6	0.2	0.8	0.3595
							1.2			0.5082
							2.0			0.6078
0.1	0.5	0.5	0.5	1.2	0.3	0.2	1.0	0.4	0.8	0.4689
								0.8		0.4712
								1.2		0.47569
0.1	0.5	0.5	0.5	1.2	0.3	0.2	1.0	0.2	1.5	0.4699
									1.7	0.4195
									1.9	0.3605

The Numerical iterations for local skin friction coefficients $-f''(0)$, $-g''(0)$, local Nusselt number $-\theta'(0)$, local Sherwood number $-\phi'(0)$ and local density number of microorganism number $-\chi'(0)$ against prominent involved parameters are discussed in Tables 1–4. Table 1 displays the result of local skin friction coefficients, $-f''(0) - g''(0)$ for parameters like λ, Nr, Nc, M, K, α, We_1 and We_2. It is found that local skin friction coefficients declines for higher variation of λ, α while grow up for Nr and Nc. From Table 2, it is observed that local Nusselt number reduces for growing variations of thermophoresis parameter Nt, buoyancy ratio parameter Nr and bioconvection Rayleigh number Nc. Table 3 witnesses that local Sherwood number $-\phi'(0)$ boosted up by increasing the magnitudes of mixed convection parameter λ and concentration relaxation parameter Ω_C. The local density number

Table 3. Numerical iteration for local Sherwood number $-\phi'(0)$ versus involved parameters.

Parameters									
λ	Nr	Nc	M	Pr	Nt	Nb	Le	Ω_C	$-\phi'(0)$
0.2	0.5	0.5	0.5	1.2	0.3	0.2	2.0	0.2	0.7068
0.6									0.7137
1.2									0.7224
0.1	0.2	0.5	0.5	1.2	0.3	0.2	2.0	0.2	0.7047
	0.6								0.7015
	1.2								0.7012
0.1	0.5	0.2	0.5	1.2	0.3	0.2	2.0	0.2	0.7040
		0.8							0.6936
		1.6							0.6775
0.1	0.5	0.5	0.1	1.2	0.3	0.2	2.0	0.2	0.7023
			0.2						0.7142
			0.3						0.7223
0.1	0.5	0.5	0.5	2.0	0.3	0.2	2.0	0.2	0.2719
				3.0					0.2939
				5.0					0.3094
0.1	0.5	0.5	0.5	1.2	0.1	0.2	2.0	0.2	0.2396
					0.5				0.1502
					1.2				0.5321
0.1	0.5	0.5	0.5	1.2	0.3	0.1	2.0	0.2	1.4092
						0.5			0.2820
						1.2			0.1175
0.1	0.5	0.5	0.5	1.2	0.3	0.2	1.0	0.2	0.7110
							1.6		0.7069
							2.2		0.7040
0.1	0.5	0.5	0.5	1.2	0.3	0.2	2.0	0.4	0.7443
								0.8	0.7546
								1.2	0.7623

of microorganism $-\chi'(0)$ enhanced for larger Peclet number Pe and bioconvection Lewis number Lb Table 4.

5. Main Findings

The effects of bioconvection on 3D hyperbolic tangent nanofluid with Cattaneo–Christov double diffusion theory, convective heat/mass conditions over a sheet are scrutinized. The nonlinear dimensionless system of mathematical model is solved with the help of famous shooting scheme. Salient traits of observation are listed as follows:

- Improving mixed convection parameter λ and Weissenberg number increases the velocity field.
- Velocity falls down versus Hartmann number and power law index parameter while it upsurges via rotation parameter.

Table 4. Numerical iteration for local microorganism density number $-\chi'(0)$ versus involved parameters.

Parameters							
λ	Nr	Nc	M	Pe	Lb	n	$-\chi'(0)$
0.2	0.5	0.5	0.5	0.1	1.0	0.1	0.6850
0.6							0.6974
1.2							0.7130
0.1	0.2	0.5	0.5	0.1	1.0	0.1	0.6814
	0.6						0.6789
	1.2						0.6740
0.1	0.5	0.2	0.5	0.1	1.0	0.1	0.6799
		0.8					0.6599
		1.6					0.6296
0.1	0.5	0.5	0.1	0.1	1.0	0.1	0.6776
			0.2				0.6554
			0.3				0.6245
0.1	0.5	0.5	0.5	0.2	1.0	0.1	0.8144
				0.6			1.1153
				1.2			1.4229
0.1	0.5	0.5	0.5	0.1	0.6	0.1	0.5119
					1.2		0.7620
					2.0		1.0453
0.1	0.5	0.5	0.5	0.1	1.0	0.2	0.6789
						0.4	0.7965
						0.8	1.1013

- For larger estimation of thermophoresis parameter and Biot number temperature of nanomaterials intensifies.
- Improvement in thermal relaxation parameter and mixed convection parameter causes reduction in thermal field of species.
- Volumetric concentration of nanoparticles upsurges with the increase of activation energy parameter E while it decreases for larger concentration relaxation parameter.
- The microorganism field declines with Peclet number and bioconvection Lewis number.

Acknowledgments

The research was supported by the National Natural Science Foundation of China (Grant Nos. 11971142, 11871202, 61673169, 11701176, 11626101, 11601485).

References

1. S. U. Choi and J. A. Eastman, *Enhancing Thermal Conductivity of Fluids with Nanoparticles* (No. ANL/MSD/CP-84938; CONF951135-29) (Argonne National Laboratory, IL United States, 1995).

2. J. Buongiorno, *ASME J. Heat Transf.* **128** (2006) 240.
3. M. Ramzan, S. Riasat, S. Kadry, C. Long, Y. Nam and D. Lu, *Appl. Sci.* **10**(1) (2020) 168.
4. I. Tlili, S. Naseer, M. Ramzan, S. Kadry and Y. Nam, *Entropy* **22**(4) (2020) 453.
5. M. Ahmad, T. Muhammad, I. Ahmad and S. Aly, *Physica A: Stat. Mech. Appl.* (2020) 124004.
6. L. A. Khan, M. Raza, N. A. Mir and R. Ellahi, *J. Therm. Anal. Calorim.* **140**(3) (2020) 879.
7. M. Kahani, *Heat Transf. Eng.* **41**(4) (2020) 377.
8. U. Ali, M. Y. Malik, A. A. Alderremy, S. Aly and K. U. Rehman, *Physica A: Stat. Mech. Appl.* (2020) 124026.
9. M. Benkhedda, T. Boufendi, T. Tayebi and A. J. Chamkha, *J. Therm. Anal. Calorim.* **140**(1) (2020) 411.
10. S. Ghahremanian, A. Abbassi, Z. Mansoori and D. Toghraie, *J. Mol. Liq.* (2020) 113310.
11. Y. Amini, S. Akhavan and E. Izadpanah, *J. Therm. Anal. Calorim.* **139**(1) (2020) 755.
12. M. Bahiraei, A. Monavari, M. Naseri and H. Moayedi, *Int. J. Heat Mass Transf.* **151** (2020) 119359.
13. N. C. Roşca, A. V. Roşca, I. Pop and J. H. Merkin, *Heat Mass Transf.* **56**(2) (2020) 547.
14. T. Muhammad, H. Waqas, S. A. Khan, R. Ellahi and S. M. Sait, *J. Therm. Anal. Calorim.* (2020) 1.
15. M. Ali, F. Sultan, W. A. Khan, M. Shahzad and H. Arif, *Chaos, Solitons Fractals* **133** (2020) 109656.
16. G. Taza, A. Khan, B. Muhammad, A. N. Aedh, M. Safyan, Z. Shah and K. Poom, *Sci. Rep. (Nature Publisher Group)* **10**(1) (2020).
17. M. R. Eid, K. L. Mahny, A. Dar and T. Muhammad, *Physica A: Stat. Mech. Appl.* **540** (2020) 123063.
18. H. A. Ogunseye, Y. O. Tijani and P. Sibanda, *Heat Transf.* **49**(6) (2020) 3374.
19. M. Faisal, I. Ahmad and T. Javed, *SN Appl. Sci.* **2**(9) (2020) 1.
20. S. Arrhenius, *Z. Phys. Chem.* **4**(1) (1889) 96.
21. A. R. Bestman, *Int. J. Energy Res.* **14**(4) (1990) 389.
22. T. Salahuddin, N. Siddique, M. Arshad and I. Tlili, *AIP Adv.* **10**(2) (2020) 025009.
23. N. S. Khan, P. Kumam and P. Thounthong, *Sci. Rep.* **10**(1) (2020) 1.
24. M. Z. Ullah, A. S. Alshomrani and M. Alghamdi, *Physica A: Stat. Mech. Appl.* **550** (2020) 124024.
25. F. E. Alsaadi, T. Hayat, M. I. Khan and F. E. Alsaadi, *Comput. Methods Programs Biomed.* **183** (2020) 105051.
26. J. R. Platt, *Science* **133** (1961) 1766e7.
27. A. V. Kuznetsov, *Int. Commun. Heat Mass Transf.* **37**(10) (2010) 1421.
28. M. Sohail, R. Naz and S. I. Abdelsalam, *Phys. Scr.* **95**(4) (2020) 045206.
29. M. M. Bhatti and E. E. Michaelides, *J. Therm. Anal. Calorim.* (2020) 1.
30. N. S. Khan, Q. Shah, A. Bhaumik, P. Kumam, P. Thounthong and I. Amiri, *Sci. Rep.* **10**(1) (2020) 1.
31. H. Waqas, S. U. Khan, M. Hassan, M. M. Bhatti and M. Imran, *J. Mol. Liq.* **291** (2019) 111231.
32. S. U. Khan, H. Waqas, M. M. Bhatti and M. Imran, *J. Non-Equilib. Thermodyn.* **45**(1) (2020) 81.

33. H. Waqas, S. U. Khan, I. Tlili, M. Awais and M. S. Shadloo, *Symmetry* **12**(2) (2020) 214.
34. S. A. Shehzad, T. Mushtaq, Z. Abbas, A. Rauf, S. U. Khan and I. Tlili, *Appl. Math. Mech.* (2020) 1.
35. B. Ali, S. Hussain, Y. Nie and I. Raza, *Phys. Scr.* (2020).
36. C. S. Balla, R. Alluguvelli, K. Naikoti and O. D. Makinde, *J. Appl. Comput. Mech.* **6**(3) (2020) 653.
37. A. Javadi, J. Arrieta, I. Tuval and M. Polin, *Philos. Trans. R. Soc. A* **378**(2179) (2020) 20190523.
38. H. Waqas, S. U. Khan, M. M. Bhatti and M. Imran, *J. Therm. Anal. Calorim.* (2020) 1.
39. H. Waqas, M. Imran, T. Muhammad, S. M. Sait and R. Ellahi, Numerical investigation on bioconvection flow of Oldroyd-B nanofluid with nonlinear thermal radiation and motile microorganisms over rotating disk.
40. Y. Wang, H. Waqas, M. Tahir, M. Imran and C. Y. Jung, *IEEE Access* **7** (2019) 130008-23.